Analysis of Superconducting Microwave Structures: Application to Microstrip Lines

Samir M. El-Ghazaly, *Senior Member, IEEE,* Robert B. Hammond, *Member, IEEE,* and Tatsuo Itoh, *Fellow, IEEE*

Abstract—**An accurate analysis for the microwave and millimeter-wave transmission lines, which include high T_c superconductor materials, is presented. This analysis is based on blending a full electromagnetic wave model with London's equations and the two-fluid model. It is capable of fully characterizing the transmission lines, including obtaining the current distributions inside the superconducting material, the electromagnetic fields, the power handling capability and the quality factor. A simplified model based on the TM-mode solution is also presented. The solution is obtained using the finite-difference scheme. This approach is employed in investigating the superconducting microstrip structure. Results showing current distributions and quality factors are presented. Variations of the line characteristics with the strip width are also presented. The possibility of developing empirical relations for the current carrying capacity as functions of the critical current density and the critical magnetic flux density is also demonstrated.**

I. Introduction

THE DISCOVERY of materials that maintain their low-loss properties at relatively high temperatures, above the liquid nitrogen boiling temperature (e.g., [1]–[3]), renewed the interest in developing practical components that exploit the promising features of the superconductivity phenomena. Such a material is normally known as high T_c superconductor (HTS). Some HTS's can be deposited in a thin film form on appropriate dielectrics, which makes them very suitable for microwave and millimeter-wave device applications. Advantages of using HTS's at high frequencies include: 1) very small losses (obviously), which means low-attenuation and low-noise; 2) very small dispersion up to frequencies of several tens of GHz [4]; 3) smaller devices due to the lower losses, which leads to larger integration density; and 4) the propagation time can be greatly reduced because of the smaller size and the shorter interconnects. Several applications of superconductors in the microwave area have already been reported (e.g., [4]–[13]).

Manuscript received June 14, 1991; revised October 22, 1991. This work was supported by the National Science Foundation under Grant ECS-9108933 to Arizona State University and by Superconductor Technologies, Inc.

S. M. El-Ghazaly is with the Department of Electrical Engineering, Arizona State University, Tempe, AZ 85287-5706.

R. B. Hammond is with Superconductor Technologies Inc., Santa Barbara, CA 93111.

T. Itoh is with the Department of Electrical Engineering, University of California, Los Angeles, Los Angeles, CA 90024-1594.

IEEE Log Number 9105701.

Before full exploitation of HTS's, several theoretical and technological problems have to be solved. On the technological side, uniform films with lower defect density, improved reproducibility, precise control over the film dimensions, and ability to directly deposit films on lower dielectric constant substrates are necessary. On the theoretical side, better understanding of the conduction mechanisms inside the superconductors is essential. The development of appropriate physical and mathematical models, which are suitable for integration with the electromagnetic theory to provide accurate representations of devices and circuits made of these materials, is urgently needed. The developed models should satisfy demands of different users and consider all aspects of the problem. For instance, the power handling capability of HTS microwave lines needs to be addressed. The maximum current density that can be carried by a superconducting material without losing its superconducting characteristics (i.e., the critical current density) depends on the critical magnetic flux density, the critical temperature, and, of course, the material itself. When an HTS is used in a transmission line, the maximum current that can be carried by the structure does not always correspond to the conductor cross-sectional area multiplied by the critical current density, since the current densities may not be uniformly distributed over in the conductor. The mathematical solutions of most, if not all, of modern planar microwave lines exhibit current and field singularities at the sharp edges of the conductors, which means that the current densities are strongly nonuniform. Therefore, the current carrying capacity of HTS microwave lines cannot be assessed without an accurate knowledge of the current and the field distributions on the line.

Considering the theoretical research developed in the field superconducting microwave transmission lines, one finds it is somewhat limited due to the young age of HTS's. The attention is mostly focused on developing expressions characterizing the transmission line in terms of integrated quantities (i.e., characteristic impedance, Q-factor, loss tangent, propagation constant . . . etc.), [14]–[29]. A brief discussion of the power handling capability of a superconductor meander line is presented in [24]. Kown *et al.* studied very high-speed system-level superconductor interconnects by neglecting fringing fields, which limits the validity of their results to very wide strip lines (i.e., quasi-parallel plate lines) [4]. Pond

and Weaver calculated field and energy density profiles in layered and superconductor-dielectric structures [26]. Again, this was for a system of parallel plates, and the current distributions were not addressed. Ghoshal and Smith extended their studies on copper to superconductor microstrip lines [17]; but again they focused on the integrated parameters. Other approaches including complex resistive boundary conditions and spectral-domain analysis were also used [28]–[29], [40]. We have come across limited number of trials for calculating current distributions in superconductors [30]–[32]. In two cases [30] and [31], the obtained results are not applicable to modern microwave lines as a result of approximations made, as it will be discussed later. In [32], only the strip line was considered, which is a TEM structure. Therefore, we believe that the power handling capability of practical HTS microwave lines has not been adequately addressed.

In this paper we will describe a direct approach for obtaining current distributions, power handling capabilities, and propagation characteristics of HTS microwave lines. The presented approach is applied to investigate the microstrip lines with emphasis on assessing their relative power handling capabilities.

II. The Theoretical Analysis

The problem at hand involves two main phenomena; the current conduction in the HTS and the electromagnetic wave propagation down the microwave transmission line. It is their interaction that we are interested in. The manner in which every mechanism influences the other determines and reshapes the constituents of each system. To model HTS microwave transmission lines, an accurate model describing the different current components as functions of the electric and magnetic fields is required. This model must be valid for the microwave band. Another model capable of predicting the electric magnetic fields inside the transmission line as functions of the material parameters, current densities and boundary conditions is also needed. The complete solution is achieved by coupling the two models. In the following sections, we will present different models that satisfy these requirements.

A. Currents in Superconductor Materials

Superconductors can be classified into two main types [33]–[34]. A Type-I superconductor, which has a coherence length larger than the penetration depth (λ), and Type-II superconductor with a coherence length much smaller than λ. The early superconducting materials, metals and alloys, were Type-I. The recently-discovered HTS materials are *considered* Type-II. They include $(La, Ba)_2CuO_4$, $YBa_2Cu_3O_7$, $Bi_2Sr_2Ca_2Cu_3O_{10}$, and $Tl_2Ba_2Ca_2Cu_3O_{10}$. The latter three materials are called YBCO, BSCCO and TBCCO respectively. Type-II superconductors are called "hard" materials. They have relatively high critical temperatures, normally above 77 K; except $(La, Ba)_2CuO_4$, which has $T_c = 35$ K. They have two values for the critical magnetic field. The lowest, below which the magnetic field is completely expelled (Meissner state), is known as H_{c1}. The second one, known as H_{c2}, describes the highest magnetic field that can be applied before the material completely losses its superconducting characteristics. For magnetic fields between H_{c1} and H_{c2} the field penetrates the superconductor and a mixed state is created, in which the material is a combination of superconducting and nonsuperconducting regions. The three families (i.e., YBCO, BSCCO and TBCCO) have been successfully deposited in thin films using currently available techniques for processing semiconductor devices (e.g.; MOCVD).

The current carrying mechanism in Type-II superconductors is considered a local phenomenon, which means that the current density at any point may be described by the local field at the same point [33]–[35]. The phenomenological two-fluid model can be used to macroscopically predict the relation between the local field and the current density. This model assumes that the conducting electrons in a superconductor are divided into two categories: superconducting electrons, known as Cooper pairs or electron pairs, and normal electrons [33]–[37]. The electron pair transport is assumed to be collision-free, while the normal electron transport is governed by the momentum conservation equation as follows;

$$m \frac{d\boldsymbol{v}_s}{dt} = -q\boldsymbol{E} \tag{1}$$

and

$$m \frac{d\boldsymbol{v}_n}{dt} + m \frac{\boldsymbol{v}_n}{\tau} = -q\boldsymbol{E}. \tag{2}$$

The total conduction current density consists of two components: the superconducting current density $\boldsymbol{J}_s$ and the normal electron density $\boldsymbol{J}_n$.

$$\boldsymbol{J} = \boldsymbol{J}_s + \boldsymbol{J}_n \tag{3}$$

where

$$\boldsymbol{J}_s = -qn_s\boldsymbol{v}_s \tag{4}$$

and

$$\boldsymbol{J}_n = -qn_n\boldsymbol{v}_n = \sigma_n\boldsymbol{E}. \tag{5}$$

The densities of superconducting and normal electrons, n_s and n_n respectively, are related to the total carrier density n and temperature T by the following relations:

$$n_s = n\left[1 - \left(\frac{T}{T_c}\right)^4\right] \tag{6}$$

and

$$n_n = n\left(\frac{T}{T_c}\right)^4. \tag{7}$$

The penetration depth (λ) variation with temperature is given by

$$\lambda(T) = \lambda(0)\left[1 - \left(\frac{T}{T_c}\right)^4\right]^{-1/2} \tag{8}$$

where $\lambda(0)$ is the penetration depth at $T = 0$.

Knowing the superconductor and the normal current densities and the structure boundary conditions, one can solve for the associated electric and magnetic fields. The losses, Q-factor and power-handling capabilities can readily be obtained.

B. Associated Electric and Magnetic Fields

Although the Meissner Effect can be interpreted to show that currents in a superconducting material can flow without electric field [33], [35], (1)–(7) demonstrate that electric field is needed for temperatures above 0 K or for ac currents even at 0 K. Moreover, the electromagnetic theory dictates that the flowing currents generate magnetic fields in dc cases, and both electric and magnetic fields in ac cases. These fields should comply with the material parameters in the structure at hand and the imposed boundary conditions. This is achieved through Maxwell's equations by appropriately introducing the superconductor characteristics through the constitutive relations. The following London's equations are used to represent the constitutive for the superconducting currents:

$$\frac{\partial \boldsymbol{J}_s}{\partial t} = \frac{1}{\mu_o \lambda^2}\boldsymbol{E}, \tag{9}$$

$$\nabla \times \boldsymbol{J}_s = \frac{-1}{\lambda^2}\boldsymbol{H}. \tag{10}$$

These equations when coupled with the two-fluid model represent the full constitutive model that describes the total current in terms of the electric and magnetic fields. It is the role of Maxwell's equations to predict the electric and magnetic fields in terms of these currents. The complete solution is achieved when the outputs of London's equations, the two-fluid model and Maxwell's equations are consistent.

C. Full-Wave Analysis

The starting point is Maxwell's equation:

$$\nabla \times \boldsymbol{H} = j\omega\epsilon\boldsymbol{E} + \boldsymbol{J}_s + \boldsymbol{J}_n. \tag{11}$$

A time dependence in the form of $e^{j\omega t}$ is understood. Substituting (5) and (9) into (11) results in

$$\nabla \times \boldsymbol{H} = \xi \boldsymbol{J}_s \tag{12}$$

where

$$\xi = -\omega^2\mu_o\epsilon\lambda^2 + j\omega\mu_o\sigma_n\lambda^2 + 1. \tag{13}$$

It is appropriate for this problem to use an auxiliary potential function to simplify the mathematical manipulation. The typical magnetic vector potential $\boldsymbol{A}$ is employed. It is defined as

$$\boldsymbol{H} = \frac{1}{\mu}(\nabla \times \boldsymbol{A}) \tag{14}$$

Equation (14) is combined with (10) to eliminate $\boldsymbol{H}$. This results in

$$\boldsymbol{J}_s = \frac{-1}{\mu_o\lambda^2}\boldsymbol{A} + \nabla\Psi \tag{15}$$

where Ψ is a scalar function to be determined from the boundary conditions. Substituting (14) and (15) into (12), one obtains

$$\nabla^2\boldsymbol{A} - \frac{\xi}{\lambda^2}\boldsymbol{A} = -\mu_o\xi\nabla\Psi \tag{16}$$

where Coulomb's gauge ($\nabla \cdot \boldsymbol{A} = 0$) was used.

Equation (16) is a distorted form of a nonhomogeneous vector wave equation. It is labeled distorted due to the term "ξ/λ^2", which is different from the conventional wave number. Equation (16) is used in the different media to describe the magnetic vector potential distribution by supplying the appropriate values of ϵ, λ and σ_n, assuming that $\mu = \mu_o$ everywhere. In the air and dielectric regions, it reduces to the conventional homogeneous vector wave equation.

D. Physical Meaning of the Function $\nabla\Psi$

Equations (15) and (16) contain a function referred to as ($\nabla\Psi$), which is directly related to the superconducting current distributions. It was heuristically related to the boundary conditions at the superconducting surfaces. The equation governing this function can be derived by substituting (15) in (11), which yields

$$\nabla \times \boldsymbol{H} = j\omega\epsilon\boldsymbol{E} - \frac{1}{\mu_o\lambda^2}\boldsymbol{A} + \nabla\Psi + \boldsymbol{J}_n. \tag{17}$$

Taking the divergence of (17), and using Coulomb's gauge and $\nabla \cdot \boldsymbol{E} = \rho/\epsilon$ yields

$$\nabla^2\Psi = -j\omega(\rho - \rho_n) \tag{18}$$

where ρ and ρ_n are the total and normal electron charge densities respectively. Equation (18) is the basic definition for the complementary part of the superconductor current density.

To gain a physical insight into and assess the importance of $\nabla\Psi$, consider the case when $\rho_n \ll \rho$, which is a reasonable assumption for superconductors at $T \ll T_c$. Also, consider a quasi-TEM wave propagation with dependence $e^{j\beta z}$, which means that $\partial/\partial x = \partial/\partial y = 0$. In this case, the current flows along the direction of the wave propagation, which is the z-direction. Only the z-component of $\nabla\Psi$ is needed. Therefore, $\nabla^2\Psi$ simplifies to

$$\nabla^2\Psi \approx \frac{\partial}{\partial z}\nabla\Psi \cdot \boldsymbol{a}_z = -j\beta\nabla\Psi \cdot \boldsymbol{a}_z, \tag{19}$$

which leads to

$$\nabla\Psi \cdot \boldsymbol{a}_z = \frac{\omega}{\beta}\rho = v_{\text{ph}}\rho \tag{20}$$

where v_{ph} is the phase velocity of the propagating wave. This shows that $\nabla\Psi$ is a two dimensional function related to the surface current density on the superconductor surface; since ρ is zero everywhere except near the surface. Due to the strong singularity exhibited by ρ at the sharp edges, this function evidently plays an important role in shaping all the current and field distributions. Muchowski *et al.* [30], and Alsop *et al.* [31] derived expressions for the current distributions in superconductors at dc. However, $\nabla\Psi$ was considered as a constant in both cases. This results in inaccurate results in both current and field distributions in microwave structures. Moreover, this leads to nonphysical results in the form of current distributions in a superconducting transmission line that are independent of the dielectric constants of the substrates. Both studies obtained results for air-filled lines at dc. Moreover, Muchowski's calculations assumed a wide and thin superconducting film, which means the error introduced by this approximation may be small. In modern microwave transmission lines employing HTS's, high dielectric constant substrates are used (e.g., $LaAlO_3$, which has $\epsilon_r \approx 18.5$ [12]). This makes the current density carried by the HTS surface facing the dielectric much larger than the current density on the air side of the strip. This phenomenon is similar to that observed in microstrip lines made of normal conductors [38]. Therefore, the above mentioned approximation, namely taking $\nabla\Psi$ as a constant, is not acceptable for modern microwave transmission lines. It is worth mentioning that sometimes this function could be approximated by a constant as, for example, the case of a very wide microstrip line over a thin substrate and a thick superconductor (i.e., $W >> d$ and $t >> \lambda$). Yet, the significance of this approximation is that the microstrip line is approximated as a parallel-plate transmission line, which is a trivial one-dimensional case. It does not require an elaborate numerical scheme to obtain its current distributions.

E. Eigenvalue or Excitation Problem?

In principle, the wave equations governing linear transmission line structures result in eigenvalue problems when discretized in a matrix form. The eigenvalues are the propagation constants and the corresponding eigenvectors are the possible modes.

In the full wave approach, described by (16), calculations of the magnetic vector potential distribution require the knowledge of both the propagation constant and the function $\nabla\Psi$. This is easily visualized by rewriting (16) in a form suitable for calculations as follows.

$$\left(\nabla_t^2 + \gamma^2 - \frac{\xi}{\lambda^2}\right)\boldsymbol{A} = -\mu_o \xi \nabla\Psi \tag{21}$$

where propagation in the form of $e^{-\gamma z}$ is assumed. It is worth mentioning that $\boldsymbol{A}$ is not exactly an eigenvector (i.e., mode) of (21) due to the presence of the source term of the right-hand side and the term "ξ/λ^2" as well. Only when both γ and the source term distribution (i.e., $\nabla\Psi$) are known, $\boldsymbol{A}$ can be obtained from (21). Hence, $\boldsymbol{A}$ is viewed to be a linear combination of two sets of solutions. The first set consists of the eigenvectors of the homogeneous wave equation resulting from substituting $\nabla\Psi = 0$ in (21). The second set is the particular solution that complies with the source term.

One should notice that the amplitudes of $\nabla\Psi$, $\boldsymbol{A}$, $\boldsymbol{E}$, $\boldsymbol{H}$, $\boldsymbol{J}_s$, $\boldsymbol{J}_n$, at any point and the total current carried by the transmission line are linearly related to each other since the model we have so far presented for the waveguiding system is linear. This is an important point in designing transmission lines. For instance, one can set the electric potential of the strip to 1 V, and use this information to calculate all the other quantities. Doubling the electric potential automatically means that all other first order quantities are doubled since, as we mentioned, the system is linear. However, this is not exactly the case in real HTS materials where the losses, or the conductivity of normal electrons σ_n, depends on the local value of the magnetic field. We will come back to this point later when we discuss effects of this nonlinearity on the transmission line characteristics.

III. Simplified Solution

The previously described approach can easily be implemented in a simplified, yet accurate, form. For typical HTS materials, $\xi \approx 1$ for frequencies up to 1000 GHz. The practical applications of HTS materials is currently limited to the microwave range, which permits us to use the "$\xi = 1$" approximation. Moreover, the practical microwave transmission lines are normally operated in their fundamental quasi-TEM mode. Actually, it is the TM mode in our case. The current flows along the direction of the wave propagation (i.e., z-direction). Therefore, only the z-component of $\boldsymbol{A}$ exists. The equation governing A_z is obtained from (16) as

$$\nabla_t^2 A_z - \frac{1}{\lambda^2} A_z = -\mu_o \nabla\Psi \cdot \boldsymbol{a}_z \tag{22}$$

inside the superconductor material, and

$$\nabla_t^2 A_z = 0 \tag{23}$$

in the air and dielectric regions. The operator ∇_t^2 is the Laplacian operator in the transverse plane (i.e., xy-plane). This is obviously a pure excitation problem. The amplitude of A_z depends on the boundary conditions and on the z-component of $\nabla\Psi$, which in turn depends on the electric field, or the applied voltage, between the strip and the ground plane. The z-component of $\nabla\Psi$ is a two-dimensional function with dependence on x and y only, since it has a propagating-wave nature along the z-direction.

Equations (22) and (23) are discretized over the transmission line cross-section using a non-uniform two-di-

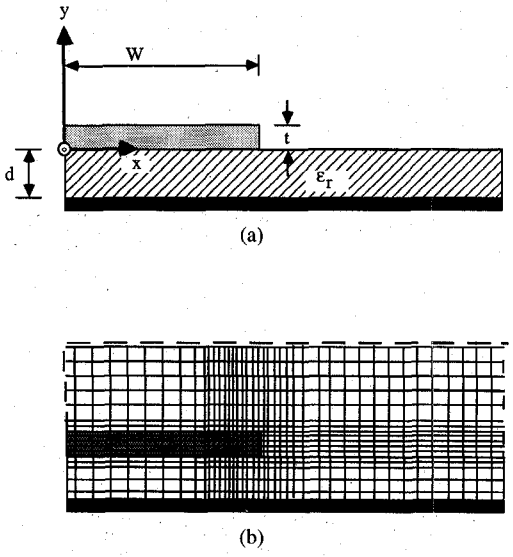

Fig. 1. (a) Simulated microstrip structure. (b) Utilized nonuniform mesh.

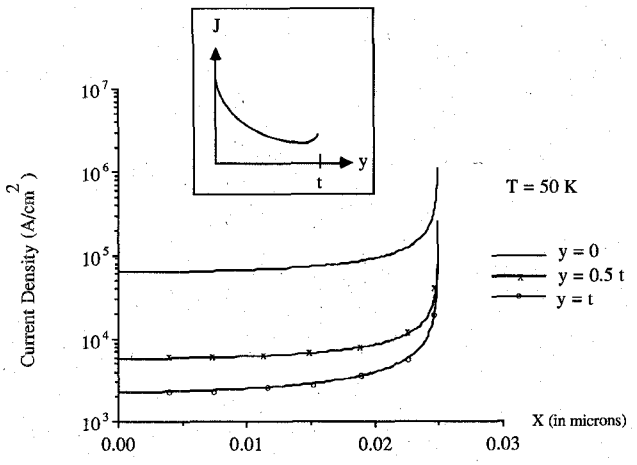

Fig. 2. Current density distributions as functions of x at constant y planes.

mensional finite difference scheme. Depending on the structure symmetry, the grid can cover only one-half of the structure as shown in the microstrip in Fig. 1. Appropriate boundary conditions should be applied. For the example shown in Fig. 1, Neumann boundary condition, which is equivalent to a magnetic wall, is applied at $x = 0$. The other open boundaries can be terminated with perfectly conducting walls, either electric or magnetic. The effects of these walls on the final solution are minimized, and practically eliminated, by placing them relatively far from the strip [39]. The upper wall may be placed $4 \sim 5$ times the dielectric thickness d, and the side wall may be placed $4 \sim 5$ times half the strip width W apart from the center.

Once the magnetic vector potential distribution inside the structure is known, (15) is used to calculate the superconducting current distribution J_s in the strip and in the ground plane, when needed. The transverse electric and magnetic field components are directly derivable from A_z. London's first equation, (9), is used to calculate the corresponding longitudinal component of the electric field. Given the normal conductivity of the material, J_n can be calculated using (5). Hence, the characteristic impedance, power and quality factors (Q) are readily calculated. The unloaded Q is defined as

$$Q = \frac{\omega(W_e + W_m)}{P_l} \tag{24}$$

where W_e and W_m are the time-average energy stored in the electric and magnetic fields per unit length of the line respectively, and P_l is the time-average power dissipated in the superconducting strip per unit length.

IV. Results and Discussion

The above mentioned simplified approach is applied to the superconducting microstrip transmission line problem shown in Fig. 1(a) with $2W = 500$ μm, $d = 425$ μm and $t = 1$ μm. The substrate is made of a loss-less dielectric material with a relative dielectric constant of 23. The superconductor is characterized by $T_c = 100$ K, the penetration depth at $T = 0$ K is $\lambda(0) = 0.18$ μm, the density of electrons is 10^{21} cm^{-3}, and the conductivity of normal electrons $\sigma_n = 10^4$ S/cm at $T = T_c$. A nonuniform two-dimensional mesh is used as shown in Fig. 1(b). The simulation region is extended to, at least, 12 W in the x-direction and to 5 d in the y-direction. Magnetic walls are used to terminate the open boundaries. Thanks to the symmetry of the structure, only one half of the microstrip line is simulated.

A. Performance Analysis

Fig. 2 shows the current density distributions inside the HTS strip as functions of x at constant y-planes, at $T = 50$ K. The total current carried by the strip is normalized to 100 mA. It is shown that the current is mainly carried by the superconductor surface adjacent to the dielectric substrate. The current decreases with the increase of y, and it slightly increases as y approaches t as schematically shown in the insert in Fig. 2. This phenomenon is due to the high dielectric constant material used in the substrate as explained in [38]. This dielectric material is chosen since it represents a typical material currently used in industry. The distribution of A_z over the transverse-plane is shown in Fig. 3. This figure is expanded to emphasize the distribution in the vicinity of the superconducting strip. The edge singularity and the large A_z on the dielectric side of the strip compared to the air side are clearly manifested.

Variations of the microstrip line characteristics with temperature can be understood by inspecting the following three figures. The current density distribution at planes $y = 0$ and $y = t$, for different temperatures, 50 K, 77 K and 89 K, is depicted in Fig. 4. The total current is normalized to 100 mA in all the three cases. It is shown that the current at $y = 0$ plane is the highest at $t = 50$ K, and decreases as the temperature increases. At the plane $y = t$, the current density is the highest at $T = 89$ K, and de-

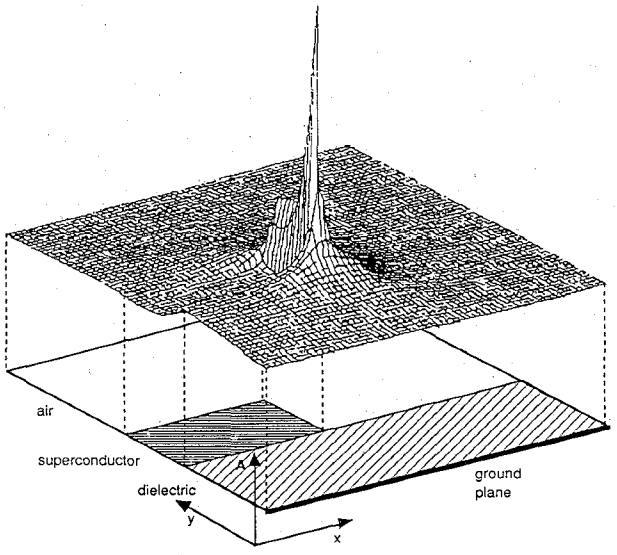

Fig. 3. Distribution of the magnetic vector potential A_z in the transverse plane.

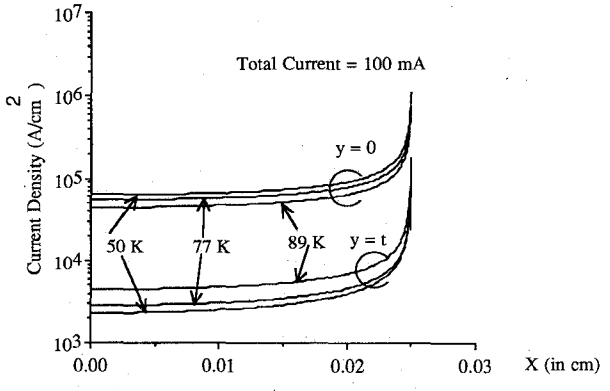

Fig. 4. Current density distributions at different temperatures.

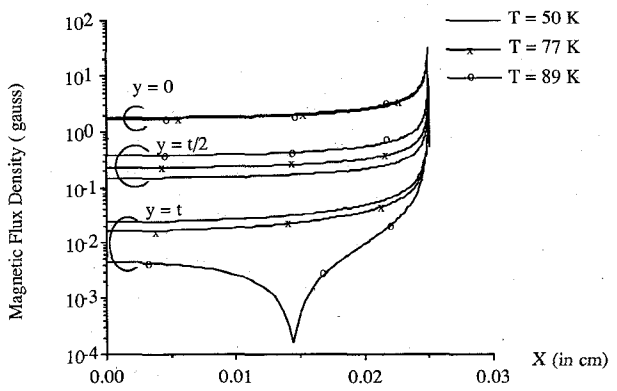

Fig. 5. Magnetic flux density distributions at different temperatures.

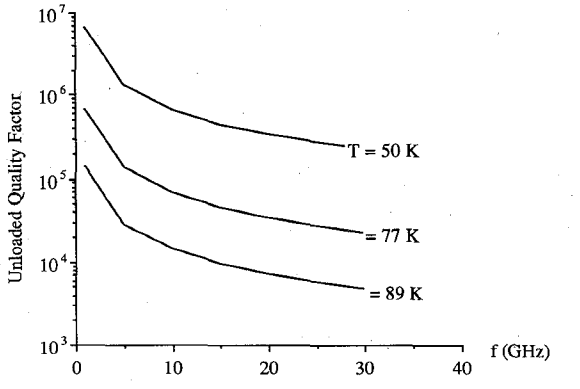

Fig. 6. Unloaded quality factor variations with frequency at different temperatures.

creases at lower temperatures. This can be explained by the increase of the penetration depth with temperature, which means that more current is carried by the core of the superconducting material. The increased ability of the superconductor to expel the magnetic field at lower temperatures is demonstrated in Fig. 5. The cases shown in Fig. 5 correspond to examples studied in Fig. 4. Bearing in mind that all the three cases carry the same total current, the $\boldsymbol{B}$ distributions at plane $y = 0$ are almost the same at the three different temperatures. However, the magnitude of $\boldsymbol{B}$ is increased at $y = t/2$ as the temperature is increased. Once again, this is due to the increase of the penetration depth with temperature. This leads to the decrease of $\boldsymbol{B}$ with the increase of temperature at $y = t$. Interesting phenomenon is observed at 89 K, when the contribution of $\boldsymbol{B}$ induced by the current at the lower surface penetrates the superconductor and opposes the $\boldsymbol{B}$ induced by the weak current at the upper surface. This phenomenon leads to the reduction of $\boldsymbol{B}$ at $x \cong 0.0145$ cm, for the $y = t$ case.

The unloaded Q of the strip is shown in Fig. 6. A monotonic decrease of the Q with frequency and temperature is shown. As expected, the Q decreases with the increase of temperature because of the increae of the normal electron density and the decrease of the number of superconducting electron pairs, as revealed by (7). However, the Q dependence on the operating temperature is not proportional to T^4, since the penetration depth also increases with temperature. The latter effect means that a larger conductor area becomes available to the current as the temperature increases. The Q dependence on the frequency can be understood by knowing that most of the energy, $(W_e + W_m)$ in (24), is stored in the dielectric regions outside the superconductor material. For the given dimensions and frequency range used, this energy is fairly independent of frequency. The power dissipated in the strip P_l is proportional to the frequency squared. Hence, the Q varies approximately as F^{-1} at a constant temperature. It should be noted that although these arguments are based on first order approximations, the results presented in Fig. 6 are based on accurate solutions of equations presented in Sections II and III.

B. Effect of the Strip Width

In this section, the effect of the strip width on the superconducting microstrip line characteristics is investigated. All the structure parameters will be kept as mentioned before, except the strip width ($2W$) is varied from

2 μm to 500 μm. This study is performed at $T = 77$ K. The superconducting current density distributions as functions of x, on the lower surface of the superconducting strip (i.e., $y = 0$) are shown in Fig. 7 for different strip widths. All of them carry a total current of 100 mA. For structures with relatively wide strips, the current density is fairly uniform over most of the strip. The current increases very rapidly near the strip edge due to the field singularity. The graph demonstrates that the ratio between the peak current density at the edge to the current density at the middle of the strip decreases as W decreases. This means that the current density becomes more uniform for smaller W. However, the current density magnitude in the middle of the strip increases as W decreases since a smaller sectional area becomes available. For strips of $W = 1$ μm, edge singularity vanishes completely. Obviously, the latter case is very similar to a wire over a ground plane, on which the current is almost uniform. One should notice that depending on the superconductor material used, the superconducting characteristics may be lost at small W due to the high current density, which may exceed the critical current density. In other words, strips of low W may not be able to carry the specified 100 mA, and as the strip width is reduced the total current has to be reduced accordingly.

Fig. 7 reveals an interesting relation between the peak current density and W. It is shown that the logarithm of the peak current density varies almost linearly with logarithm of W. An empirical relation can be derived, which is very useful for CAD. Taking this structure as a case study, this relation becomes

$$J_{\text{peak}} = 1.202 \times 10^5 \exp [0.53758 \ln (W)] \quad \text{A/cm}^2 \tag{25}$$

where W is in cm. This equation is derived with a total current of 100 mA. The maximum error resulting from using (25), relative to the numerical calculations, is about 5%. The actual current carrying capacity can be deduced from (25) thanks to linearity of the model. Given the material critical current density J_c (in A/cm^2),the maximum current that can be carried by the shown structure is given by

$$I_{\max} = 8.3187 \times 10^{-4} J_c \exp [0.53758 \ln (W)] \quad \text{mA.} \tag{26}$$

The magnetic flux density $\boldsymbol{B}$ is another important factor, which must be considered in the design of HTS microwave structures. To avoid losing the superconducting characteristics of the material, the magnitude of $\boldsymbol{B}$ inside the HTS strip should not exceed the critical value B_c. Therefore to complete the design procedure, $\boldsymbol{B}$ distributions must be obtained as well. Fig. 8 illustrates the $\boldsymbol{B}$ distributions for the cases depicted in Fig. 7 at the same total current of 100 mA. These distributions obtained at $y = 0$, which represents the surface of the highest magnetic field. Once again, B shows a strong singularity at the strip edges. It is also observed that the logarithm of the peak

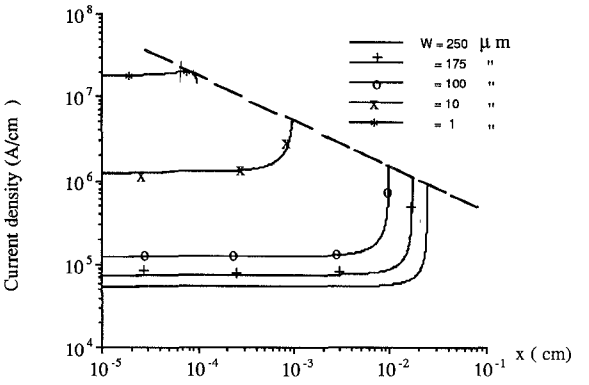

Fig. 7. Current density distributions at the superconductor-dielectric interface for devices of different widths carrying a total current of 100 mA.

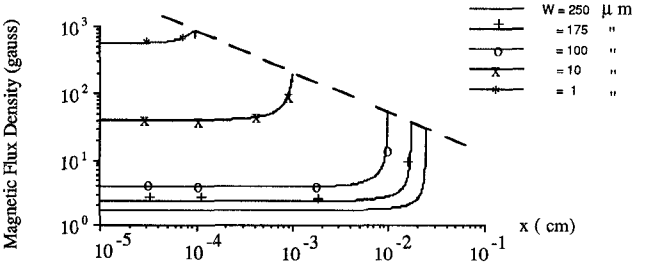

Fig. 8. Magnetic flux density distribution at the superconductor-dielectric interface for devices of different widths carrying a total current of 100 mA.

B varies almost linearly with logarithm of W on the logarithmic scale of Fig. 8. This enables the derivation of an empirical relation between the strip width and B_{peak} as follows.

$$B_{\text{peak}} = 3.254 \exp [-0.60046 \ln (W)] \quad \text{gauss} \tag{27}$$

where W is in cm. An expression estimates the current carrying capacity as a function of the strip width and B_c (in gauss), similar to (2), is also developed as follows:

$$I_{\max} = 30.731 B_C \exp [0.60046 \ln (W)] \quad \text{mA.} \tag{28}$$

In designing HTS transmission lines, both eq. (26) and (28) must be used simultaneously. The smallest of the resulting two currents is the correct line capacity.

The variations of the Q with the strip width, at different frequencies, are shown in Fig. 9. It is interesting to notice that the Q is very high at very small strip widths. This is because the current density distributions becomes more uniform, in the x-direction, at small W as shown in Fig. 7. As W is increased, the Q decreases due to the increased importance of the edge singularity. For a relatively large W (i.e., $W > 200$ μm) the Q saturates. The latter phenomenon is understood by knowing that increasing W eventually leads to a more uniform current near the center of the strip; and the current singularities at the edges do not change significantly. Of course, the Q decreases at high frequencies, as shown in Fig. 9, because of the higher electric field inside the superconductor, which leads to higher losses.

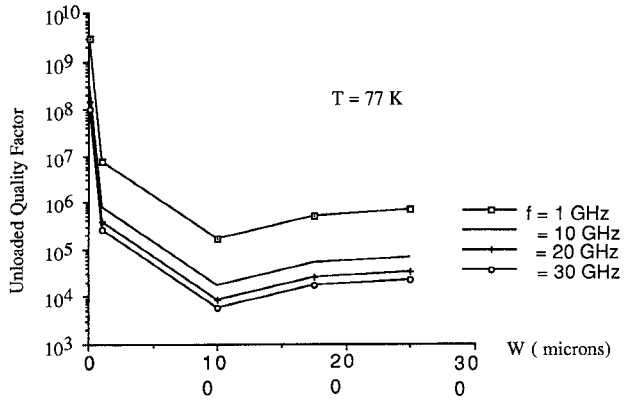

Fig. 9. Variations of the unloaded quality factor with the strip width at different frequencies.

C. Practical Considerations

The approach and the results presented here are very interesting from practical point of view, and will have a considerable impact on the design and applications of the HTS.

Based on the results shown in Fig. 2, it is expected that the ratio of the current carried by the upper surface to the current carried by the lower surface increases by using a lower dielectric constant substrate. This indicates that lower dielectric constant substrates lead to a more uniform current distributions, which increases the current carrying capacity of the line.

The characteristics revealed in Figs. 7–9 indicated that there are two ranges of dimensions that can be used depending on the application. The first one is the narrow strip (e.g., $2W \leq 20$ μm). In this range the current distribution tends to be more uniform, which leads to a high Q as shown in Fig. 9. However, the total current carried by such a device is limited, as demonstrated by (26), due to the small cross-sectional area of the superconductor. This range can be utilized in applications that require very high Q and involve very small currents, such as resonators for low-noise amplifiers. The second range is for wide strip (e.g., $2W \geq 400$ μm), in which the effect of the edge singularity becomes less critical. Therefore, increasing W increases the total current carried by the line without significantly affecting the Q. This range is very useful for applications that require high current carrying capacity, while the Q is not crucial. It is useful to know that increasing W beyond certain value, about 200 μm in this case, does not degrade the Q when all other parameters are kept constant. However, before fully exploiting the results of Fig. 9, one should recall that loss-less substrates are used. The very high field generated by the high current densities for small strip widths may significantly alter these results due to the high dielectric loses in the substrates. Also, the nonlinearities of the HTS material may drastically affect the Q vaues at small W.

The empirical relations developed in (26) and (28) are of significant importance from CAD point of view. It is understood that these equations do not represent the ultimate effort in this direction. Obviously, comprehensive study is required to include the dependence of these expressions on the other parameters including on the strip thickness, the substrate thickness, and dielectric constant. Nevertheless, the aim of this paper is to report the calculated results, and to indicate that the derivation of empirical relations is possible based on an accurate numerical analysis. Future research in this direction should be encouraged.

In the presented model, the normal electron conductivity in HTS was taken as a constant parameter. However, our preliminary results show that a strong magnetic field exists at the HTS strip corners. Such a strong field can lead to either a loss of the superconductivity property or a reduction of the superconducting current relative to the normal current, which is considered as a partial loss of the superconductivity. This will have a substantial effect on the losses in the superconductor and the Q of the line. Theoretically, this converts the problem from a relatively complicated *linear* transmission line system into a *nonlinear* one, and immediately cripples the applicability of most of the standard transmission line approaches. On the other hand, the power and the flexibility of our proposed approach manifests itself in handling this problem. Consider the normal conductivity to be a function of the local magnetic flux density as

$$\sigma_n(B) = \sigma_{n0} + \sigma_{n1}(B) \tag{29}$$

where $\sigma_{n1}(B)$ accounts for the dependence of the conductivity on $\boldsymbol{B}$. Such a nonlinear conductivity model can be very easily incorporated in our model, and should be used in the future when more accurate results are needed.

V. Conclusion

A theoretical analysis for HTS microwave transmission lines is presented. It is based on a full-wave analysis, London's equations and the two-fluid model. An accurate, yet flexible, approach is described. A simplified solution technique based on the TM mode is suggested, implemented, and applied to the superconducting microstrip structure. The results indicate that the use of a high dielectric constant material in the substrate accumulates the current on one side of the strip, which drastically reduces the current carrying capacity. The choice of the optimal strip width should be based on the desired Q and total current to be carried by the line. It is also shown that deriving empirical relations to be used in CAD design of HTS microwave lines is possible. Finally, our investigation reveals that there is an urgent need for an accurate study that sets the standards for the design of HTS microwave transmission lines taking into account all the practical aspects of the problem.

Nomenclature

- $\boldsymbol{A}$ Magnetic vector potential.
- $\boldsymbol{B}$ Magnetic flux density.
- $\boldsymbol{E}$ Electric field intensity.

$\boldsymbol{H}$ Magnetic field intensity.
j $\sqrt{-1}$.
$\boldsymbol{J}$ Total conduction current density.
$\boldsymbol{J}_n$ Normal electron current density.
$\boldsymbol{J}_s$ Superconducting current density.
m Electron mass.
n Number of electrons per unit volume.
n_n Number of normal electrons per unit volume.
n_s Number of superconducting electrons per unit volume.
P_l Time-average power dissipated in the superconducting strip.
q Electron charge.
t Time.
T Temperature.
T_c Critical temperature of the superconductor.
v_n Average velocity of normal electrons.
v_{ph} Phase velocity of the propagating wave.
v_s Average velocity of superconducting electrons.
W_e Time-average energy stored in the electric field.
W_m Time-average energy stored in the magnetic field.
ϵ Permittivity.
λ The penetration depth of the superconductor.
τ Momentum relaxation time.
μ Permeability.
ω Angular frequency ($= 2\pi f$, where f is the frequency).
ρ Volumetric charge density.
σ Conductivity.
σ_n Conductivity of normal electrons.
σ_s Conductivity of superconducting electrons.

ACKNOWLEDGMENT

The authors would like to thank S. Strazdus for generating Fig. 3, and D. Scalapino for interesting discussions and suggestions.

REFERENCES

[1] M. K. Wu *et al.*, "Superconductivity at 93 K in a new mixed-phase Y-Ba-Cu-O compound system at ambient pressure," *Phys. Rev. Lett.*, vol. 58, no. 9, pp. 908–910, 1987.

[2] J. Sun *et al.*, "Superconductivity and magnetism in the high-T_c superconductor Y-BaCu-O," *Phys. Rev. lett.*, vol. 58, no. 15, pp. 1574–1576, 1987.

[3] R. J. Cava *et al.*, "Bulk superconductivity at 91 K in single phase oxygen-deficient perovskite $Ba_2YCu_3O_{9-\delta}$," *Phys. Rev. Lett.*, vol. 58, no. 16, pp. 1676–1679, 1987.

[4] O. Kown, B. Langley, R. Pease, and M. Beasley, "Superconductors as very high-speed system-level interconnects," *IEEE Electron Device Lett.*, vol. EDL-8, no. 12, pp. 582–585, 1987.

[5] C.-S. Pao, Y. Li, and S.-P. Chou, "A superconducting-dielectric resonator at W-bands," in *IEEE MTT-S Int. Microwave Symp. Dig.*, 1988, pp. 457–458.

[6] H. Chaloupka, G. Muller, U. Klein, and H. Piel, "New experimental results for microwave conductivity of high-TC superconductors and consequences for applications to linear devices," in *IEEE MTT-S Int. Microwave Symp. Dig.*, 1989, pp. 547–550.

[7] L. Hornak *et al.*, "Experiments with a 31-cm High-T_c Superconducting Thin Film Tranmission Line," in *IEEE MTT-S Int. Microwave Symp. Dig.*, 1989, pp. 623–626.

[8] D. Oates, A. Anderson, and B. Shih, "Superconducting Stripline Resonators and High-T_c materials," in *IEEE MTT-S Int. Microwave Symp. Dig.*, 1989, pp. 627–630.

[9] J. Konopka *et al.*, "Microwave detectors based on granular high-T_c thin films," in *IEEE MTT-S Int. Microwave Symp. Dig.*, 1989, pp. 635–638.

[10] J. Martens *et al.*, "A superconducting single film device oscillator made of high Tc and low Tc materials," in *IEEE MTT-S Int. Microwave Symp. Dig.*, 1989, pp. 443–446.

[11] R. Dill *et al.*, "Testchip for high temperature superconductor passive devices," in *IEEE MTT-S Int. Microwave Symp. Dig.*, 1990, pp. 863–866.

[12] R. B. Hammond *et al.*, "Superconducting Tl-Ca-Ba-Cu-O thin film microstrip resonator and its power handling performances at 77 K," in *IEEE MTT-S Int. Microwave Symp. Dig.*, 1990, pp. 867–870.

[13] R. Bernetti and A. Williams, "Preliminary design steps for thin-film superconducting filters," in *IEEE MTT-S Int. Microwave Symp. Dig.*, 1990, pp. 273–276.

[14] J. Pond and C. Krowne, "Slow-Wave Properties of Superconducting Microstrip Transmission Lines," in *IEEE MTT-S Int. Microwave Symp. Dig.*, 1988, pp. 449–452.

[15] B. Young and T. Itoh, "Loss Reduction in Superconducting Microstrip-Like Transmission Lines," in *IEEE MTT-S Int. Microwave Symp. Dig.*, 1988, pp. 453–456.

[16] J. F. Whitaker *et al.*, "Propagation model for ultrafast signals on superconducting dispersive striplines," *IEEE Trans. Microwave Theory Tech.*, vol. 36, no. 2, pp. 277–285, 1988.

[17] U. Ghoshal and L. Smith, "Skin effects in narrow copper microstrip at 77 K," *IEEE Trans. Microwave Theory Tech.*, vol. 36, no. 12, pp. 1788–1795, 1988.

[18] D. McGinnis and J. Beyer, "A broad-band microwave superconducting thin-film transformer," *IEEE Trans. Microwave Theory Tech.*, vol. 36, no. 11, pp. 1521–1525, 1988.

[19] L. Drabeck *et al.*, "Surface impedance of high T_c superconductors," in *IEEE MTT-S Int. Microwave Symp. Dig.*, 1989, pp. 551–554.

[20] J. Pond, P. Weaver and I. Kaufman, "Propagation characteristics of inductively-coupled superconducting microstrip," in *IEEE MTT-S Int. Microwave Symp. Dig.*, 1989, pp. 451–454.

[21] C. Hilbert, D. Gibson, and D. Herrell, "A comparison of lossy and superconducting interconnect for computers," *IEEE Trans. Electron Devices*, vol. 36, no. 9, pp. 1830–1839, 1989.

[22] H.-Y. Lee and T. Itoh, "Phenomenological loss equivalence method for planar quasi-TEM transmission lines with a thin normal conductor or superconductor," *IEEE Trans. Microwave Theory Tech.*, vol. 37, no. 12, pp. 1904–1909, 1989.

[23] H. Chaloupka, N. Klein, and S. Orbach, "Effect of finite thickness on the surface impedance of high T_c thin films," in *IEEE MTT-S Int. Microwave Symp. Dig.*, 1990, pp. 855–858.

[24] A. Fathy *et al.*, "Microwave properties and modeling of high-T_c superconductor thin film meander line," in *IEEE MTT-S Int. Microwave Symp. Dig.*, 1990, pp. 859–862.

[25] K. B. Bhasin *et al.*, "Performance and modeling of superconducting ring resonators at millimeter-wave frequencies," in *IEEE MTT-S Int. Microwave Symp. Dig.*, 1990, pp. 269–272.

[26] J. Pond and P. Weaver, "Field and energy-density profiles in layered superconductor-dielectric structures," in *IEEE MTT-S Int. Microwave Symp. Dig.*, 1990, pp. 277–280.

[27] T. van Deventer *et al.*, "High frequency characterization of high-temperature superconducting thin film lines," in *IEEE MTT-S Int. Microwave Symp. Dig.*, 1990, pp. 285–288.

[28] J. Pond, C. Krowne, and W. Carter, "On the application of complex resistive boundary conditions to model transmission lines consisting of very thin superconductors," *IEEE Trans. Microwave Theory Tech.*, vol. 37, no. 1, pp. 181–190, 1989.

[29] S. Withington and E. Kollberg, "Spectral-domain analysis of harmonic effects in superconducting quasiparticle mixers," *IEEE Trans. Microwave Theory Tech.*, vol. 37, no. 1, pp. 231–238, 1989.

[30] E. Muchowski and A. Schmid, "On the current distribution in a shielded superconducting film," *Z. Physik*, 255, pp. 187–195, 1972.

[31] L. Alsop, A. Goodman, F. Gustavson, and W. Miranker, "A numerical solution of a model for a superconductor field problem," *J. Computational Physics*, vol. 31, pp. 216–239, 1979.

[32] D. Sheen, S. Ali, D. Oates, R. Withers, and J. Kong, "Current distributions in superconducting strip transmission lines," in *IEEE MTT-S Int. Microwave Symp. Dig.*, Boston, MA, 1991.

[33] T. Van Duzer and C. W. Turner, *Principles of Superconductive Devices and Circuits*. New York: Elsevier, 1981.

[34] R. E. Matick, *Transmission Lines for Digital and Communication Networks*. New York: McGraw-Hill, 1969.

[35] F. London, *Superfluids*. New York: Wiley, vol. 1, 1950.

[36] P. Mason and R. Gould, "Slow-wave structures utilizing superconducting thin-film transmission lines," *J. Appl. Phys.*, vol. 40, no. 5, pp. 2039–2051, 1969.
[37] J. Swihart, "Field solution for a thin-film superconducting strip transmission strip transmission line," *J. Appl. Phys.*, vol. 32, no. 3, pp. 461–469, 1961.
[38] S. El-Ghazaly, T. Itoh, and R. Hammond, "Design considerations for high T_c superconductor microstrip lines based on current distributions," *Microwave and Optical Tech. Lett.*, July 1991.
[39] E. Yamashita, "Variational method for the analysis of microstrip-like transmission lines," *IEEE Trans. Microwave Theory Tech.*, vol. 16, no. 8, pp. 529–535, 1968.
[40] C.-W. Kuo and T. Itoh, "An iterative method for the nonlinear characterization of the high T_c Superconducting Microstrip Lines," in *Proc. European Microwave Conf.*, Stuttgart, Germany, Sept. 1991.

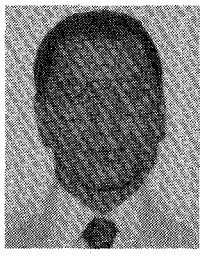

Samir M. El-Ghazaly (S'84–M'88–SM'91) was born in Egypt, on July 1, 1959. He received the B.Sc. degree in electronics and communications engineering (Distinction, Honors) in 1981, and the M.Sc. degree in 1984, both from Cairo University, Cairo, Egypt, and the Ph.D. degree, in electrical engineering, from the University of Texas at Austin, in 1988.

In October 1981 he was appointed as a Teaching Assistant in the Department of Electronics and Communication Engineering, Cairo University, and became Assistant Lecturer in 1984. From November 1982 to October 1983, he was with the Centre Hyperfrequences et Semiconducteurs, Université de Lille I, Lille, France. He worked on the simulation of the submicron-gate MESFET's. In January 1984, he joined the Department of Electrical Engineering, University of Ottawa, Canada, where he worked on the analysis of *E*-plane circuits. In September 1986, he joined the Department of Electrical and Computer Engineering at the University of Texas at Austin as a research assistant first and became a Post-Doctoral Fellow in 1988. In September 1988, he joined Arizona State University as an Assistant Professor. His research interests include microwave and millimeter-wave semiconductor devices and passive circuits, semiconductor device simulations, ultra-short pulse propagation, superconductor microwave transmission lines, wave-device interactions, electromagnetics, and numerical techniques applied to monolithic microwave integrated circuits.

Dr. El-Ghazaly is a member of Tau Beta Pi, Sigma Xi, Eta Kappa NU, and an elected member of Commission D of URSI. He is on the Editorial Board of the IEEE TRANSACTIONS ON MICROWAVE THEORY AND TECHNIQUES, and is the Chairman of the IEEE-Waves and Devices Group, Phoenix Section.

Robert B. Hammond (M'79), photograph and biography not available at the time of publication.

Tatsuo Itoh (S'69–M'69–SM'74–F'82), for a photograph and biography, see this issue, p. 481.